

# Improvise, Adapt, Overcome — Telescopic Adapters for Efficient Fine-tuning of Vision Language Models in Medical Imaging

Ujjwal Mishra<sup>1</sup> Vinita Shukla<sup>1</sup> Praful Hambarde Amit Shukla

Centre for Artificial Intelligence and Robotics, Indian Institute of Technology Mandi, India

ujjwalmishra238@gmail.com, {d23097@students., praful@, amitshukla@}iitmandi.ac.in

## Abstract

Adapting Vision Language Segmentation Models (VLSMs) to medical imaging domains requires significant computational overhead when using conventional fine-tuning approaches. Existing Parameter-Efficient Fine-Tuning (PEFT) methods apply uniform adapter dimensions across all transformer layers, leading to suboptimal parameter allocation and reduced adaptation efficiency. We introduce Telescopic Adapters, a novel PEFT framework that employs depth-aware scaling to progressively increase adapter capacity from shallow to deep transformer layers. Our method integrates lightweight bottleneck modules within CLIPSeg’s vision and text encoders, with adapter dimensions dynamically scaled based on layer depth and semantic relevance. Using only 613k trainable parameters—244× fewer than end-to-end fine-tuning, Telescopic Adapters achieve superior performance across five diverse medical datasets spanning polyp segmentation, skin lesion detection, and breast ultrasound imaging. Comprehensive ablation studies demonstrate that deeper layers require substantially more adaptation capacity than shallow layers, validating our telescopic scaling hypothesis. Our approach establishes a new paradigm for efficient medical VLSM fine-tuning, enabling deployment in resource-constrained clinical environments while maintaining competitive segmentation accuracy.

## 1. Introduction

Medical image segmentation is a dense prediction task that involves labeling each pixel in an image to identify anatomical structures or areas affected by disease [41]. With the increasing use of computer-aided diagnosis (CAD) in the last decade [9], it has become an important tool in diagnosis [11], treatment planning [15], and accurate patient monitoring [12]. The success of deep learning in CAD [50, 56] has translated into substantial improvements

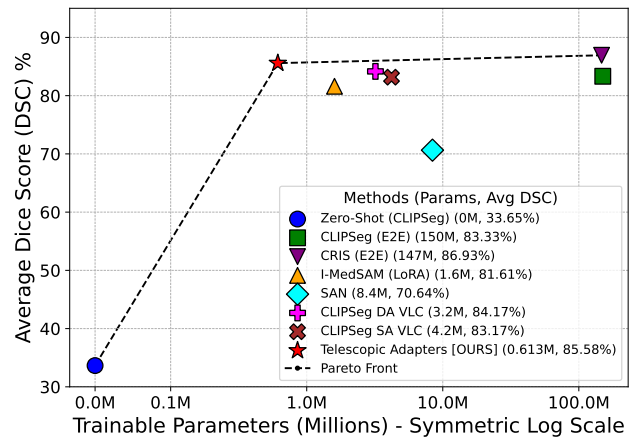


Figure 1. Performance vs. Parameter Efficiency plot. Average Dice Score (DSC %) across five datasets is plotted against the number of trainable parameters (in millions) on a symmetric log scale. Our method (Telescopic Adapters) and other parameter-efficient approaches are compared against End-to-End (E2E) fine-tuning and a Zero-Shot baseline. The dashed line indicates the Pareto front, showing the optimal trade-off between performance and parameter cost.

in medical image segmentation models across diverse imaging modalities, anatomies, and diseases [31]. However, these models are typically trained on specific foreground classes and imaging modalities, limiting their adaptability to new images or additional information sources [5]. Scaling up data for specific segmentation tasks remains challenging due to high costs of data collection and annotation [16], posing challenges for real-world clinical deployment where imaging protocols and diagnostic needs vary widely.

Recent efforts have explored incorporating textual information as auxiliary supervision to overcome these limitations [6]. Medical images are frequently accompanied by textual reports containing detailed descriptions of anatomical structures, pathological findings, and spatial relations.

<sup>1</sup>These authors contributed equally.

These text-based cues complement visual information, particularly when annotations are scarce or image quality is suboptimal [28]. Vision Language Models (VLMs), such as CLIP [39], have emerged as powerful foundations for multimodal approaches. CLIP employs contrastive loss on large-scale image-text pairs to align semantically related embeddings in a shared representation space. Building on these capabilities, VLMSs [14] extend VLMs to dense prediction tasks. CLIPSeg [32] combines frozen CLIP encoders with lightweight transformer-based decoders for open-vocabulary segmentation, while Yu *et al.* [48] leverage CLIP with self-supervised mask proposal networks for zero-shot referring image segmentation.

Although these models achieve impressive results in open domains [32, 42, 57], their zero-shot performance on medical image segmentation remains limited. This performance gap necessitates fine-tuning VLMSs on domain-specific medical datasets to effectively capture clinical semantics and imaging characteristics [55]. However, conventional fine-tuning of large-scale VLMs, often comprising hundreds of millions to billions of parameters, is computationally expensive and memory intensive [20]. Such resource demands pose significant challenges for deployment in clinical environments, particularly in low-resource or mobile settings. Parameter-Efficient Fine-Tuning (PEFT) methods address these limitations by adapting pretrained models through modifying only a small fraction of parameters. Among widely adopted PEFT techniques are Adapters [22] and Low-Rank Adaptation (LoRA) [23]. Adapter-based methods insert lightweight, trainable modules within frozen model backbones, enabling task-specific adaptation with minimal computational overhead. Adapter strategies have been explored more extensively than LoRA in vision-language contexts, making them particularly relevant for VLMSs [13]. To address these limitations, we introduce *Telescopic Adapters* for fine-tuning VLMSs on medical image segmentation. Our approach augments CLIPSeg with learnable adapter modules and a depth-aware scaling mechanism that progressively increases adapter capacity from shallow to deep layers. Using only 613k trainable parameters— $244\times$  fewer than E2E fine-tuning—our method outperforms existing parameter-efficient approaches as shown in Fig 1. The main contributions of this work are:

- We introduce novel telescopic adapter modules with depth-aware scaling for fine-tuning VLMSs to domain-specific smaller datasets using minimal learnable parameters.
- Our experiments and results on medical datasets with diverse modalities indicate that our telescopic adaptation strategy outperforms both end-to-end fine-tuning and existing PEFT methods for VLMSs.

- We provide comprehensive studies on Adapter dimensions and positioning, demonstrating that progressive scaling and strategic placement result in superior performance with minimal parameter overhead.

## 2. Related Work

### 2.1. Vision Language Models

Vision language models (VLMs) have shown notable progress, enabling cross-modal understanding spanning diverse vision tasks [47, 49]. CLIP [39], trained on large-scale image-text pairs, has demonstrated strong generalization and zero-shot capabilities [17]. Open source model such as the OpenCLIP implementation [24] have further supported large-scale pretraining and reproducibility. Beyond classification, CLIP-based models have been applied to tasks that involve region segmentation and classification through text-driven supervision [18]. These developments have motivated extensions into the medical domain. Models such as PubMedCLIP [10] and MedCLIP [43] incorporate biomedical text corpora and improve CLIP alignment in clinical contexts. Other variants [44] introduce self-supervised learning, cross-view consistency, and domain-specific enhancements to improve zero-shot performance in low-resource medical environment. Among these, BiomedCLIP [53] demonstrates strong performance in multiorgan retrieval and classification tasks.

Building on the success of CLIP, recent VLMSs aim to take advantage of textual prompts for dense prediction tasks. CLIPSeg [32] enhances CLIP’s architecture by introducing a lightweight transformer decoder that fuses vision and text representations to enable prompt-driven segmentation. Unlike retrieval-based methods, CLIPSeg supports both zero-shot and fine-tuned segmentation scenarios and accommodates ViT backbones. In contrast, Wang *et al.* [42] formulates segmentation as a region retrieval problem, employing a CNN-based CLIP vision encoder to align visual features with textual queries. While CRIS [42] has shown promise in localizing relevant regions, its reliance on a convolutional backbone limits scalability and integration with modern transformer-based pipelines. BiomedCLIPS [53] further extends this direction by adapting its encoders for segmentation, though it lacks an E2E pretrained decoder and hence is typically used with task-specific fine-tuning.

### 2.2. Parameter Efficient Fine Tuning

The increasing scale of VLMs has improved cross-modal generalization across a wide range of visual tasks. However, these models are predominantly trained on broad open-domain datasets and often underperform when applied to specialized domains such as medical imaging. Domain adaptation strategies address this limitation by transferring knowledge from a source domain to a target domain,

typically with limited supervision [54]. Conventional approaches include unsupervised domain adaptation through pseudo-labeling [58], style transfer [8], or contrastive and adversarial learning [40], while more recent work explores test time and online adaptation for dynamic deployment scenarios [36]. Despite their flexibility, these methods frequently incur considerable computational cost and instability during inference.

Given the prohibitive cost of retraining large-scale models in full, PEFT has emerged as an effective alternative for adapting VLMs to downstream tasks with minimal computational burden. PEFT methods reduce training and memory costs by updating only a small subset of parameters, leaving the majority of pretrained model weights frozen [29]. These methods can be broadly classified into four categories: selective tuning, adapters, prompt-based tuning, and low-rank adaptation. Selective tuning methods restrict optimization to specific components within the architecture. Ben *et al.* [2] fine-tunes only the bias terms of the attention and feedforward layers, while other approaches apply structured pruning to derive task-specific subnetworks [21].

Adapter-based tuning introduces small trainable modules into the frozen backbone to modulate intermediate representations. These modules are typically lightweight bottleneck architectures inserted between transformer sublayers [22]. Adapter tuning has shown effectiveness in vision language tasks [7], enabling modular transfer and multitask learning. Variants such as CLIP-Adapter [13] adapt pretrained features through learned visual pathways that integrate both adapted and original representations. However, insertion of an adapter increases the number of model parameter inferences, which may lead to higher latency. Recent efforts aim to address this drawback through compression and adapter fusion techniques [37].

Prompt tuning replaces manually designed prompts with learnable embeddings. Initially applied to language models, this approach has been extended to vision-language settings by optimizing prompts or visual tokens [26]. These tunable embeddings, when prepended to inputs or injected into intermediate layers, steer the model toward domain-relevant behavior with minimal parameter updates. Prompt tuning is particularly attractive for few-shot and zero-shot settings [33].

Low-Rank Adaptation (LoRA) [23] represents another class of PEFT, where trainable low-rank matrices are injected into linear projections of the frozen model to capture task-specific weight updates. By design, LoRA allows for merging the adapted parameters with the original weights before inference, resulting in no additional latency or memory usage. LoRA assumes task-specific modifications reside in a low-dimensional subspace, enabling efficient fine-tuning. LoRA extension includes rank-adaptive variants [51], improved optimization strategies [4, 27], and

quantized versions to reduce memory consumption. Wei *et al.* [45] introduces LoRA to medical image segmentation paradigm for continual learning. Despite its efficiency, LoRA’s performance can be sensitive to the choice of rank and may underperform on tasks requiring more expressive adaptation, especially in high-variance domains like medical imaging.

### 3. The Proposed Method

As shown in Fig. 2 (a), we extend the CLIPSeg architecture by introducing lightweight adapter modules within the transformer encoders of both the vision and text branches, as well as a conditional adapter after the text projection. Adapters are selectively inserted into transformer layers at positions preceding residual addition, allowing localized modulation of representations at both attention and feed-forward sublayers as shown in Fig. 2 (b). Each adapter is designed as a bottleneck projection with a learnable residual scaling parameter to control its influence on the layer output. To improve adaptation efficiency, we introduce *teleoscopic adaptation* strategy to dynamically adjust the dimension of the adapter between layers based on their depth and relevance to the task. Deeper layers, which encode higher-level semantic representations, are assigned progressively larger bottleneck dimensions, while early layers receive minimal capacity to reduce redundancy (see Fig. 2 (d)). Finally, we append a lightweight CNN layer with 2 layers and only 48 trainable parameters after the CLIPSeg decoder. This module enhances spatial refinement of the segmentation mask without introducing significant computational overhead.

#### 3.1. Adapter Placement

We integrate lightweight adapter modules selectively across the vision, text, and conditional pathways to enable efficient and localized task-specific adaptation. These adapters are inserted within the transformer encoder blocks of the model without modifying the pretrained backbone weights as shown in Fig. 2 (a).

Let  $\mathcal{A}_v$ ,  $\mathcal{A}_t$ , and  $\mathcal{A}_c$  denote the adapters in the vision, text, and conditional branches, respectively. Each adapter  $\mathcal{A}_n$  is inserted in the  $n^{th}$  transformer encoder layer  $\mathcal{L}_n$  of its corresponding modality. Adapters are applied before each residual addition point in  $\mathcal{L}_n$ , resulting in two adapter applications per encoder layer: once after the multi-head self-attention sublayer and once after the feed-forward MLP sublayer as shown in Fig. 2 (b). This placement ensures that task-specific modulation occurs before residual addition [22].

**Vision Adapters** ( $\mathcal{A}_v$ ) are inserted into the first nine transformer layers  $\{\mathcal{L}_1, \mathcal{L}_2, \dots, \mathcal{L}_9\}$ . CLIPSeg utilizes only the intermediate representations of these layers within its decoder, and as such, adapting these specific layers allows

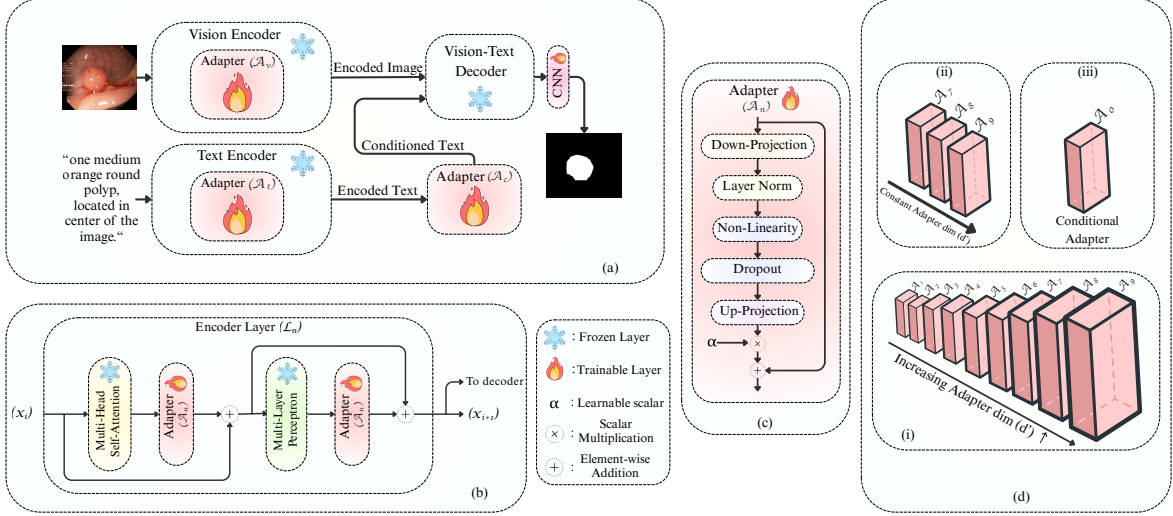


Figure 2. Overview of the proposed telescopic adaptation framework. (a) Overall architecture of the modified CLIPSeg model with integrated adapter modules. (b) Placement of adapters within the encoder branch, inserted after the multi-head self-attention and MLP sublayers. (c) Proposed adapter formulation, where the learnable scalar  $\alpha$  regulates the contribution of the adapter at each layer. (d) Telescopic Adapters across different modalities: (i) Vision branch, (ii) Text branch, and (iii) Conditional branch, illustrating progressive dimension allocation and selective adaptation.

the model to progressively adjust the visual features passed to the decoder. Each layer is augmented with two adapter modules placed before the two residual connections, resulting in 18 adapter instances on the vision encoder. This configuration ensures that each encoder block refines its activation before passing it both to the decoder and to the next layer in the stack [32].

**Text Adapters** ( $\mathcal{A}_t$ ) are inserted into the final three layers:  $\mathcal{L}_7$ ,  $\mathcal{L}_8$  and  $\mathcal{L}_9$ . These layers capture the most semantically rich and task-relevant features, making them ideal for lightweight adaptation. Earlier layers, which primarily encode syntactic and general-purpose features, are left unaltered to avoid unnecessary interference. As with the vision encoder, each selected text layer contains two adapters, one after multi-head self-attention sublayer and one after the feed-forward MLP sublayer, totaling six  $\mathcal{A}_t$  modules in the text pathway.

**Conditional Adapter** ( $\mathcal{A}_c$ ) is applied once to the output of the text encoder after projection. This adapter enables minimal but targeted transformation of the final joint text representation before it is passed to the decoder, supporting a better alignment between the textual context and the segmentation objective.

This selective and structured placement leverages the encoder-decoder architecture of CLIPSeg, ensuring that only the most relevant layers are adapted to suit the downstream dense prediction task.

### 3.2. Adapter Formulation

Building on the formulation introduced in [22], we design an adapter module that introduces non-linearity, di-

mensionality compression, and task-specific flexibility into the network without modifying the pretrained backbone as presented Fig.2 (c). The adapted representation is computed as:

$$\mathbf{f}' = \mathbf{f} + \alpha \cdot \mathbf{W}_{\text{up}} (\text{Dropout} (\sigma (\text{Norm} (\mathbf{W}_{\text{down}} \cdot \mathbf{f})))) \quad (1)$$

Here,  $\mathbf{f} \in \mathbb{R}^{\dots \times d}$  represents the input feature from the pretrained model, and  $\mathbf{f}' \in \mathbb{R}^{\dots \times d}$  is the adapted output. The transformation is defined by a bottleneck structure, where  $\mathbf{W}_{\text{down}} \in \mathbb{R}^{d \times d'}$  reduces the dimensionality and  $\mathbf{W}_{\text{up}} \in \mathbb{R}^{d' \times d}$  projects it back to the original space. The bottleneck dimension ( $d'$ ) is defined as the following inside the adapter:

$$d' = \max(8, \min(d_{\text{adapter}}, \frac{d}{4})) \quad (2)$$

We compute  $d_{\text{adapter}}$  on a per-layer basis to maintain efficiency and expressiveness. A detailed discussion on this adaptive choice is presented in the next section. The compressed features are then normalized along the feature dimension to ensure stable gradient propagation, followed by a *SiLU* activation function, which introduces smooth, input-aware non-linearity particularly suited to compact transformation layers [52]. Then a fixed rate *dropout* ( $p = 0.1$ ) is applied to regularize the transformation and reduce overfitting.

We also introduce a learnable scalar parameter  $\alpha \in \mathbb{R}$ , initialized to 0.1. This small initial value is crucial for training stability, as it ensures the untrained adapter's random weights do not destabilize the pretrained model's representations at the start of fine-tuning. This residual scaling allows the model to softly regulate the extent of task-specific

adaptation at each layer. Importantly, it also improves the interpretability of the adaptation mechanism, as higher values of  $\alpha$  reflect layers where the adapter contributes more prominently.

### 3.3. Telescopic Adaptation

To improve parameter efficiency and adaptivity, we introduce a telescopic adaptation mechanism that modulates the adapter size across transformer layers based on their depth and functional importance. Rather than employing uniform adapter widths throughout the network, this strategy assigns smaller bottleneck dimensions to early layers and progressively increases the capacity toward deeper layers.

Transformer encoders follow a coarse-to-fine representational hierarchy. The early layers predominantly capture low-level or syntactic features, while the deeper layers encode more abstract task-specific semantics [35]. Imposing large adapters on all layers uniformly not only adds redundancy but may also destabilize training. We address this by dynamically computing the per-layer adapter dimension  $d_{\text{adapter}}$  from a base value  $d_{\text{base}} = 64$ , which we empirically select to balance expressiveness and stability. Larger values were found to cause gradient explosion in the early stages of training.

**Vision Adapters.** Let  $\mathcal{L}_v$  denote the number of visual encoder layers with  $\mathcal{A}_v$ . For the  $i^{\text{th}}$  layer ( $1 \leq i \leq \mathcal{L}_v$ ), we scale the adapter dimension progressively with depth using a layer-dependent factor:

$$d_{\text{adapter}}^{(v,i)} = \max \left( 8, \left\lfloor \frac{1}{2} \cdot d_{\text{base}} \cdot \frac{i}{\mathcal{L}_v} \right\rfloor \right) \quad (3)$$

This formulation ensures a minimal adapter width of 8 and gradually increases the dimensionality to support richer adaptation in deeper layers where features are more task-relevant.

**Text Adapters.** In contrast to vision, we restrict adaptation in the text encoder to its final three layers, which carry semantically rich embeddings crucial to conditioning. Here, we opt for a statically reduced adapter dimension across all three layers:

$$d_{\text{adapter}}^{(t)} = \max \left( 8, \left\lfloor \frac{d_{\text{base}}}{4} \right\rfloor \right) \quad (4)$$

This design imposes a smaller adapter dimension of 16, reflecting the relative stability and abstraction of late-stage language representations without incurring unnecessary overhead.

**Conditional Adapter.** The conditional adapter, applied after the text projection stage, is configured with an even smaller dimension:

$$d_{\text{adapter}}^{(c)} = \max \left( 16, \left\lfloor \frac{d_{\text{base}}}{8} \right\rfloor \right) \quad (5)$$

This conservative allocation minimizes interference while allowing for controlled, task-aware modulation of the final joint text embedding before it is passed to the decoder.

The resulting adapter dimensions are then passed to the formulation in Eq. (2), where they are further bounded by the input size  $d$  to ensure stability.

## 4. Experiments

### 4.1. Datasets and Evaluation Metrics

To evaluate the effectiveness of our proposed approach, we utilize a diverse collection of medical imaging datasets spanning multiple domains, including both radiology and non-radiology modalities. Following Poudel *et al.* [38], we adopt their predefined dataset splits and corresponding text prompts to ensure consistency and comparability in performance benchmarking. Their method generates multiple text prompts per image-mask pair; in our implementation, we randomly select one prompt per sample to construct image-mask-text triplets for evaluation across datasets.

For non-radiology tasks, we utilized three polyp segmentation datasets from endoscopic images: *Kvasir – SEG* [25], *ClinicDB* [3], and *BKAI* [34]. We also included the skin lesion segmentation (*ISIC – 16* [19]) dataset for skin cancer detection. For radiology, the breast ultrasound image segmentation dataset (*BUSI* [1]) was used.

We evaluated the overall performance of the methods using the Dice Similarity Coefficient (DSC %) and Intersection over Union (IoU %), with values averaged across each dataset for the three random seed values. All metrics were computed using the MONAI framework<sup>1</sup>.

### 4.2. Implementation Details

The training and inference processes for both the baseline and proposed methods were carried out on an NVIDIA RTX A4000 GPU. Mixed-precision training with floating-point 16 was used, employing a batch size of 32. The initial learning rate for the adapter network is set to  $1 \times 10^{-3}$ . A scheduler reduced the learning rate by a factor of 0.3 if no decrease in validation loss was observed over 5 consecutive epochs. Training was stopped early if the validation DSC (%) did not improve in 20 consecutive epochs. All models were optimized using AdamW [30] with a weight decay of  $1 \times 10^{-3}$ . Each experiment was repeated with three different random seed values to assess consistency and account for variability in prompt sampling. The loss function combined Dice and binary cross-entropy losses as shown in Eq. (6) where scalar values  $\lambda_d$  and  $\lambda_{BCE}$  are set to be 1.5 and 1.

$$L = \lambda_d \cdot L_{\text{Dice}} + \lambda_{BCE} \cdot L_{\text{BCE}} \quad (6)$$

<sup>1</sup><https://monai.io>

### 4.3. Telescopic Adapter Analysis

To validate the effectiveness of our proposed telescopic adaptation strategy, we perform a comprehensive analysis of the learned adapter parameters after convergence of training. This analysis examines the evolution of the scale parameters  $\alpha$  in the vision and text branches and their distribution across layers to empirically verify the hypothesis that deeper transformer layers require more substantial task-specific adaptation. Fig. 2 (d) illustrates the telescopic design: the vision branch (i) uses progressively larger adapter dimensions across layers, the text branch (ii) applies constant dimensions in higher layers, and the conditional branch (iii) employs a single compact adapter after text projection.

Layer	Adapter Dim	Attention Scale ( $\alpha_A^V$ )	MLP Scale ( $\alpha_{MLP}^V$ )
1	8	0.0465	0.0725
2	8	0.0532	0.0905
3	10	0.0788	0.1067
4	14	0.0880	0.1145
5	17	0.0778	0.0956
6	21	0.0866	0.0982
7	24	0.1098	0.1328
8	28	0.0764	0.1164
9	32	0.0949	0.1150

Table 1. Layer-wise adapter configurations and learned scale parameters in the vision branch, showing the assigned adapter dimensionality and the final Attention ( $\alpha_A^V$ ) and MLP ( $\alpha_{MLP}^V$ ) scaling factors after training convergence.

Layer	Adapter Dim	Attention Scale ( $\alpha_A^T$ )	MLP Scale ( $\alpha_{MLP}^T$ )
7	16	0.0816	0.1061
8	16	0.1063	0.0924
9	16	0.0962	0.1070

Table 2. Layer-wise adapter configurations and learned scale parameters in the text branch, showing the assigned adapter dimensionality and the final attention ( $\alpha_A^T$ ) and MLP ( $\alpha_{MLP}^T$ ) scaling factors after training convergence.

#### 4.3.1 Scale Parameter Evolution and Regularization

The learned scale parameters were effectively regularized during training. In the vision branch (Table 1),  $\alpha_A^V$  and  $\alpha_{MLP}^V$  range from 0.046 to 0.133, while in the text branch (Table 2),  $\alpha_A^T$  and  $\alpha_{MLP}^T$  lie between 0.082 and 0.107. In the vision branch, 12 out of 18 values converged below the initialization threshold of 0.1, while six exceeded it, indicating targeted, high-impact adaptation in specific layers. In the text branch, 3 out of 6 values fell below this threshold, while three surpassed it. On average, the vision parameters show a reduction of 0.81% from their initial value, whereas the text parameters show a smaller mean reduction of 0.17%. This controlled convergence pattern suggests that the

scaling mechanism successfully modulated adaptation and maintained stability, confirming the robustness of our residual scaling formulation in Eq.( 2).

#### 4.3.2 Layer-wise Contribution Patterns

The vision branch exhibits distinct patterns consistent with the telescopic adaptation hypothesis. Early layers (1–3) have lower scales, with  $\alpha_A^V$  ranging from 0.046 to 0.079 and  $\alpha_{MLP}^V$  from 0.072 to 0.107, confirming that shallow layers require minimal task-specific modification. Deeper layers show elevated scales, with  $\mathcal{L}_7$  reaching the maximum values of  $\alpha_A^V = 0.110$  and  $\alpha_{MLP}^V = 0.133$ . This indicates that deeper layers capture more task-relevant information.

#### 4.3.3 Telescopic Dimension Effectiveness

The correlation between adapter dimension allocation and learned scales supports the telescopic design.  $\mathcal{L}_7$ , with an assigned dimension of 24 (Eq. 3), shows the highest adaptation in both  $\alpha_A^V$  and  $\alpha_{MLP}^V$ . Early layers with small dimensions (e.g.,  $\mathcal{L}_1, \mathcal{L}_2$ ) correspondingly show low scales, confirming that conservative allocation prevents unnecessary parameter usage in shallow layers.

#### 4.3.4 Attention versus MLP Adaptation

In the vision branch,  $\alpha_{MLP}^V$  consistently exceeds  $\alpha_A^V$ , with  $\alpha_{MLP}^V / \alpha_A^V$  ratio ranging from 1.13 ( $\mathcal{L}_6$ ) to 1.70 ( $\mathcal{L}_2$ ), averaging 1.36. This suggests that MLP sublayers are more critical for task-specific adaptation than attention sublayers in dense prediction tasks. In the text branch, adaptation is limited to the last three layers, but unlike the vision branch, the relationship between  $\alpha_A^T$  and  $\alpha_{MLP}^T$  is inconsistent. For example,  $\alpha_{MLP}^T$  dominates in  $\mathcal{L}_7$  and  $\mathcal{L}_9$ , while  $\alpha_A^T$  is higher in  $\mathcal{L}_8$  ( $\alpha_A^T = 0.106$  vs.  $\alpha_{MLP}^T = 0.092$ ). This suggests that in language processing, the relative contribution of attention versus MLP adaptation varies depending on the layer’s role.

#### 4.3.5 Parameter Efficiency Validation

Across both modalities, scale value ( $\alpha$ ) for 15 out of 24 (12 in vision, 3 in text) adapters converged to values below the initialization threshold ( $\alpha = 0.10$ ), demonstrating that the approach avoided over-parameterization. The nine values exceeding the threshold (6 in vision, 3 in text) represent meaningful adaptations that correlate with improved performance, indicating the model emphasized the most task-critical representations.

Overall, this analysis confirms that telescopic adaptation selectively emphasizes semantically critical layers while maintaining parameter efficiency through conservative scaling in less critical regions, validating the coarse-to-fine representational hierarchy underlying our approach.

## 4.4. Ablation Studies

### 4.4.1 Ablation Study Over Adapter Placement

Datasets	Metric	Adapter Configurations		
		• [498k]	•• [593k]	••• [613k]
Kvasir-SEG [25]	DSC (%)	87.35	89.67	<b>89.79</b>
	IoU (%)	80.32	<b>83.62</b>	83.50
BKAI [34]	DSC (%)	85.53	87.09	<b>88.38</b>
	IoU (%)	77.77	80.00	<b>81.63</b>
ClinicDB [3]	DSC (%)	85.39	91.28	<b>91.67</b>
	IoU (%)	78.45	84.85	<b>85.19</b>
ISIC-16 [19]	DSC (%)	91.61	<b>92.24</b>	92.18
	IoU (%)	85.30	<b>86.16</b>	86.12
BUSI [1]	DSC (%)	<b>70.35</b>	64.33	65.90
	IoU (%)	<b>62.45</b>	57.26	59.10

Table 3. Ablation study on adapter placement across five datasets. The configurations shown are: Vision only branches (•), Vision and Text branches (••), and Vision, Text, and Conditional branches (•••). Values in brackets correspond to the total number of trainable parameters per configuration. Best results for each metric are in **bold**.

To validate the contribution of each component in our architecture, we conduct an ablation study on adapter placement. The results in Table 3 assess the performance of three models: 1) With adapters in the vision branch only (•), 2) With adapters in the vision and text branches (••), and 3) our full model incorporating adapters in the vision, text, and conditional branches (•••).

The addition of text adapters (••) to the vision branch baseline (•) provides a substantial performance uplift across most datasets, underscoring the importance of textual context. For example, on the ClinicDB [3] dataset, this addition improves the DSC from 85.39% to 91.28% and the IoU from 78.45% to 84.85%.

Our proposed model (•••), which includes the conditional branch, consistently delivers the best or most competitive performance. This final component adds further refinement for a minimal parameter overhead of only 20k, achieving the highest scores for both metrics on the BKAI [34] and ClinicDB datasets. Which confirms that the conditional adapters effectively harmonize the features from the vision and text branches.

Notably, for the BUSI [1] dataset, the vision branch baseline (•) yields the best results. This suggests that for certain datasets with less complex inter-modal dependencies, the additional branches may not provide a benefit. However, the superior performance of the three (*i.e.* Vision, Text, and Conditional) branches model on approximately four out of five diverse datasets validates it as the most robust and effective configuration, offering an optimal balance between

parameter efficiency and high generalization capability.

## 4.5. Comparison to State-of-the-Art Methods

We evaluate our Telescopic Adapters against a zero-shot baseline and multiple fine-tuning approaches across five medical datasets, as shown in Table 4. Fig. 3 provides qualitative comparisons showing segmentation masks across representative samples from all datasets. The comparison includes E2E fine-tuning methods, LoRA-based adaptation, and existing adapter-based approaches, demonstrating significant performance and efficiency improvements.

CLIPSeg [32] (150M parameters) serves as our baseline VLSM, extending CLIP’s vision-language capabilities to segmentation tasks. Its zero-shot performance, however, is substantially low (e.g., 53.42% DSC on Kvasir-SEG), establishing a baseline that highlights the need for adaptation. While E2E fine-tuned CLIPSeg achieves competitive performance across datasets (87.69% DSC on Kvasir-SEG, 91.88% DSC on ISIC-16), it requires updating the entire parameter space. CRIS [42] (147M parameters) employs a CNN-based CLIP encoder for region retrieval-based segmentation, achieving strong results particularly on BKAI (92.62% DSC) and ClinicDB (93.63% DSC). However, CRIS’s convolutional encoder is incompatible with adapter insertion, necessitating E2E fine-tuning and limiting its efficiency for resource-constrained deployment.

Parameter-efficient approaches offer substantial computational savings while maintaining competitive performance. I-MedSAM [45] (1.6M parameters) combines frequency and LoRA adapters within the SAM framework. Despite its efficiency, I-MedSAM shows mixed results across datasets, achieving 88.05% DSC on BKAI but only 61.52% on BUSI. SAN [46] (8.4M parameters) attaches a parallel ViT network to frozen CLIP encoders, modeling segmentation as region recognition with mask proposal and attention bias branches. However, SAN demonstrates poor performance, with particularly low scores on BKAI (66.26% DSC) and BUSI (45.61% DSC), suggesting limited effectiveness for medical domain adaptation.

Existing adapter methods for VLSMs include CLIPSeg Dense Adapter (DA-VLC, 3.2M) and Shallow Adapter (SA-VLC, 4.2M) variants [6], which apply uniform adaptation across vision, text, and conditioning pathways without depth-aware scaling. CLIPSeg DA-VLC achieves consistent performance across datasets (89.06% DSC on Kvasir-SEG, 92.02% DSC on ISIC-16), while SA-VLC shows slightly lower performance (86.80% DSC on Kvasir-SEG, 91.55% DSC on ISIC-16). Both methods require significantly more parameters than our approach while achieving inferior results. As shown in Fig. 3, our Telescopic Adapters produce segmentation masks that closely align with ground truth across diverse medical imaging modalities, demonstrating superior qualitative performance compared to ex-

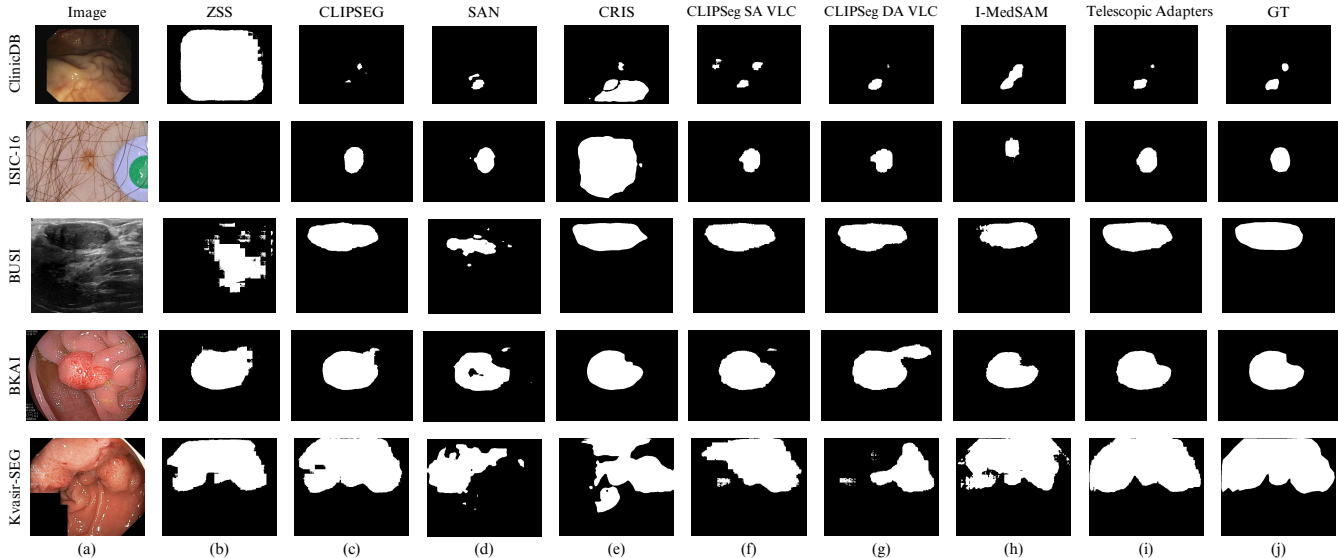


Figure 3. Segmentation results on samples from ClinicDB [3], ISIC-16 [19], BUSI [1], BKAI [34], and Kvasir-SEG [25] datasets (rows 1-5 respectively). Column (a) shows the original medical images, followed by segmentation masks from: (b) ZSS (zero-shot segmentation using CLIPSeg [32]), (c) CLIPSeg [32] (E2E fine-tuned), (d) SAN [46], (e) CRIS [42] (E2E fine-tuned), (f) CLIPSeg SA VLC [6], (g) CLIPSeg DA VLC [6], (h) I-MedSAM [45], (i) Telescopic Adapters, and (j) GT (ground truth).

Dataset	Metric	Zero-Shot	End-to-End fine-tuning		LoRA Fine-Tuning	Adapter Fine-Tuning			
		CLIPSeg [32] 150M	CLIPSeg [32] 150M	CRIS [42] 147M	I-MedSAM [45] 1.6M	SAN [46] 8.4M	CLIPSeg DA VLC [6] 3.2M	CLIPSeg SA VLC [6] 4.2M	Telescopic Adapters [OURS] 613k
Kvasir-SEG [25]	DSC (%)	53.42	87.69	89.43	86.36	69.58	89.06	86.80	<b>89.79</b>
	IoU (%)	42.48	81.72	83.37	78.66	58.05	82.28	79.33	<b>83.50</b>
BKAI [34]	DSC (%)	30.08	85.59	92.62	88.05	66.26	87.17	83.95	<b>88.38</b>
	IoU (%)	23.96	77.52	88.30	80.87	54.58	79.74	75.61	<b>81.63</b>
ClinicDB [3]	DSC (%)	36.58	88.58	93.63	88.12	81.36	89.63	89.04	<b>91.67</b>
	IoU (%)	27.54	81.51	88.74	79.91	72.61	82.89	81.95	<b>85.19</b>
ISIC-16 [19]	DSC (%)	25.15	91.88	91.49	84.00	90.39	92.02	91.55	<b>92.18</b>
	IoU (%)	20.85	85.76	85.41	75.10	83.61	85.90	85.22	<b>86.12</b>
BUSI [1]	DSC (%)	23.01	62.91	67.50	61.52	45.61	62.95	64.52	<b>65.90</b>
	IoU (%)	20.32	55.52	60.90	56.47	35.27	54.95	56.88	<b>59.10</b>

Table 4. Quantitative benchmark of segmentation performance across five medical datasets: Kvasir-SEG [25], BKAI [34], ClinicDB [3], ISIC-16 [19], and BUSI [1]. We compare our Telescopic Adapters (OURS) against: (i) the Zero-Shot (ZS) baseline (CLIPSeg [32]), (ii) End-to-End (E2E) fine-tuning (CLIPSeg [32], CRIS [42]), (iii) LoRA-based tuning (I-MedSAM [45]), and (iv) other adapter-based methods (SAN [46], CLIPSeg DA/SA VLC [6]). Performance is reported in DSC (%) and IoU (%). Parameter counts shown for PEFT methods and End-to-End fine-tuning are trainable; for Zero-Shot segmentation, they are the total model parameters.

isting methods.

## 5. Conclusion

In this work, we introduced Telescopic Adapters, a parameter-efficient fine-tuning technique that adapts vision language segmentation models to medical imaging domains using only 0.4% of the baseline model’s parameters. Our approach demonstrates competitive performance to end-to-end fine-tuning while significantly outperforming existing PEFT methods across multiple medical datasets. Our comprehensive analysis reveals that strategic adapter placement and progressive dimension scaling enable efficient domain transfer with minimal computational overhead. The learned

scale parameters empirically confirm that shallow layers require minimal changes to their learned embeddings, while deeper transformer layers benefit from increased adaptation capacity for task-specific semantic understanding. This paradigm opens pathways to continual learning and multi-task learning frameworks for VLSMs, where specialized adapters can be trained for new datasets or tasks while keeping the core architecture frozen to prevent forgetting. Such adaptability is particularly valuable for medical image segmentation, where datasets are often limited in size and diverse in imaging modalities. We encourage researchers to build upon this work and explore the broader applications of telescopic adapters across various domains and computer vision tasks.

## References

- [1] Walid Al-Dhabyani, Mohammed Gomaa, H.M. Khaled, and Aly Fahmy. Dataset of breast ultrasound images. *Data in Brief*, 28:104863, 11 2019. [5](#), [7](#), [8](#)
- [2] Elad Ben Zaken, Yoav Goldberg, and Shauli Ravfogel. Bit-Fit: Simple parameter-efficient fine-tuning for transformer-based masked language-models. In Smaranda Muresan, Preslav Nakov, and Aline Villavicencio, editors, *Proceedings of the 60th Annual Meeting of the Association for Computational Linguistics (Volume 2: Short Papers)*, pages 1–9, Dublin, Ireland, May 2022. Association for Computational Linguistics. [3](#)
- [3] Jorge Bernal, F Javier Sánchez, Gloria Fernández-Esparrach, Debora Gil, Cristina Rodríguez, and Fernando Vilariño. Wm-dova maps for accurate polyp highlighting in colonoscopy: Validation vs. saliency maps from physicians. *Computerized medical imaging and graphics*, 43:99–111, 2015. [5](#), [7](#), [8](#)
- [4] Arnav Chavan, Zhuang Liu, Deepak Gupta, Eric Xing, and Zhiqiang Shen. One-for-all: Generalized loRA for parameter-efficient fine-tuning, 2024. [3](#)
- [5] Xiaoyang Chen, Hao Zheng, Yuemeng Li, Yuncong Ma, Liang Ma, Hongming Li, and Yong Fan. Versatile medical image segmentation learned from multi-source datasets via model self-disambiguation. In *Proceedings of the IEEE/CVF Conference on Computer Vision and Pattern Recognition*, pages 11747–11756, 2024. [1](#)
- [6] Manish Dhakal, Rabin Adhikari, Safal Thapaliya, and Bishesh Khanal. Vlsm-adapter: Finetuning vision-language segmentation efficiently with lightweight blocks. In *International Conference on Medical Image Computing and Computer-Assisted Intervention*, pages 712–722. Springer, 2024. [1](#), [7](#), [8](#)
- [7] Guanliang Dong, Zhangquan Wang, Yourong Chen, Yuliang Sun, Hongbo Song, Liyuan Liu, and Haidong Cui. An efficient segment anything model for the segmentation of medical images. *Scientific Reports*, 14(1):19425, 2024. [3](#)
- [8] Aysegul Dundar, Ming-Yu Liu, Ting-Chun Wang, John Zedlewski, and Jan Kautz. Domain stylization: A strong, simple baseline for synthetic to real image domain adaptation. *arXiv preprint arXiv:1807.09384*, 2018. [3](#)
- [9] Ayman El-Baz, Garth M. Beache, Georgy Gimel’farb, Kenji Suzuki, Kazunori Okada, Ahmed Elnakib, Ahmed Soliman, and Behnoush Abdollahi. Computer-aided diagnosis systems for lung cancer: Challenges and methodologies. *International Journal of Biomedical Imaging*, 2013(1):942353, 2013. [1](#)
- [10] Sedigheh Eslami, Christoph Meinel, and Gerard de Melo. PubMedCLIP: How much does CLIP benefit visual question answering in the medical domain? In Andreas Vlachos and Isabelle Augenstein, editors, *Findings of the Association for Computational Linguistics: EACL 2023*, pages 1181–1193, Dubrovnik, Croatia, May 2023. Association for Computational Linguistics. [2](#)
- [11] Jeffrey Fauw, Joseph Ledsam, Bernardino Romera-Paredes, Stanislav Nikolov, Nenad Tomasev, Sam Blackwell, Harry Askham, Xavier Glorot, Brendan O’Donoghue, Daniel Visentin, George Driessche, Balaji Lakshminarayanan, Clemens Meyer, Faith Mackinder, Simon Bouton, Kareem Ayoub, Reena Chopra, Dominic King, Alan Karthikesalingam, and Olaf Ronneberger. Clinically applicable deep learning for diagnosis and referral in retinal disease. *Nature Medicine*, 24, 09 2018. [1](#)
- [12] Bruce Fischl, David Salat, Evelina Busa, Marilyn Albert, Megan Dieterich, Christian Haselgrove, Andre Kouwe, Ron Killiany, David Kennedy, Shuna Klaveness, Albert Montillo, Nikos Makris, Bruce Rosen, and Anders Dale. Whole brain segmentation: Automated labeling of neuroanatomical structures in the human brain. *Neuron*, 33:341–55, 02 2002. [1](#)
- [13] Peng Gao, Shijie Geng, Renrui Zhang, Teli Ma, Rongyao Fang, Yongfeng Zhang, Hongsheng Li, and Yu Qiao. Clip-adapter: Better vision-language models with feature adapters. *International Journal of Computer Vision*, 132(2):581–595, 2024. [2](#), [3](#)
- [14] Yachun Gao, Jia Guo, Chuanji Fu, Yan Wang, and Shimin Cai. Vlsm-net: A fusion architecture for ct image segmentation. *Applied Sciences*, 13(7):4384, 2023. [2](#)
- [15] Yunhe Gao, Rui Huang, Yiwei Yang, Jie Zhang, Kainan Shao, Changjuan Tao, Yuanyuan Chen, Dimitris N Metaxas, Hongsheng Li, and Ming Chen. Focusnetv2: Imbalanced large and small organ segmentation with adversarial shape constraint for head and neck ct images. *Medical Image Analysis*, 67:101831, 2021. [1](#)
- [16] Yunhe Gao, Zhiqiang Tang, Mu Zhou, and Dimitris Metaxas. Enabling data diversity: efficient automatic augmentation via regularized adversarial training. In *International conference on information processing in medical imaging*, pages 85–97. Springer, 2021. [1](#)
- [17] Gabriel Goh, Nick Cammarata, Chelsea Voss, Shan Carter, Michael Petrov, Ludwig Schubert, Alec Radford, and Chris Olah. Multimodal neurons in artificial neural networks. *Distill*, 6(3):e30, 2021. [2](#)
- [18] Xiuye Gu, Tsung-Yi Lin, Weicheng Kuo, and Yin Cui. Open-vocabulary object detection via vision and language knowledge distillation. In *International Conference on Learning Representations*, 2022. [2](#)
- [19] David Gutman, Noel CF Codella, Emre Celebi, Brian Helba, Michael Marchetti, Nabin Mishra, and Allan Halpern. Skin lesion analysis toward melanoma detection: A challenge at the international symposium on biomedical imaging (isbi) 2016, hosted by the international skin imaging collaboration (isic). *arXiv preprint arXiv:1605.01397*, 2016. [5](#), [7](#), [8](#)
- [20] Stefan Hinterstoisser, Vincent Lepetit, Paul Wohlhart, and Kurt Konolige. On pre-trained image features and synthetic images for deep learning. In *Proceedings of the European Conference on Computer Vision (ECCV) Workshops*, pages 0–0, 2018. [2](#)
- [21] Connor Holmes, Minjia Zhang, Yuxiong He, and Bo Wu. Nxmtransformer: Semi-structured sparsification for natural language understanding via admn. *Advances in neural information processing systems*, 34:1818–1830, 2021. [3](#)
- [22] Neil Houlsby, Andrei Giurgiu, Stanislaw Jastrzebski, Bruna Morrone, Quentin De Laroussilhe, Andrea Gesmundo, Mona Attariyan, and Sylvain Gelly. Parameter-efficient transfer

- learning for nlp. In *International conference on machine learning*, pages 2790–2799. PMLR, 2019. 2, 3, 4
- [23] Edward J Hu, Yelong Shen, Phillip Wallis, Zeyuan Allen-Zhu, Yuanzhi Li, Shean Wang, Lu Wang, Weizhu Chen, et al. Lora: Low-rank adaptation of large language models. *ICLR*, 1(2):3, 2022. 2, 3
- [24] Gabriel Ilharco, Mitchell Wortsman, Ross Wightman, Cade Gordon, Nicholas Carlini, Rohan Taori, Achal Dave, Vaishaal Shankar, Hongseok Namkoong, John Miller, Han-naneh Hajishirzi, Ali Farhadi, and Ludwig Schmidt. Openclip, July 2021. If you use this software, please cite it as below. 2
- [25] Debesh Jha, Pia H Smedsrud, Michael A Riegler, Pål Halvorsen, Thomas De Lange, Dag Johansen, and Håvard D Johansen. Kvasir-seg: A segmented polyp dataset. In *International conference on multimedia modeling*, pages 451–462. Springer, 2019. 5, 7, 8
- [26] Menglin Jia, Luming Tang, Bor-Chun Chen, Claire Cardie, Serge Belongie, Bharath Hariharan, and Ser-Nam Lim. Visual prompt tuning. In *Computer Vision – ECCV 2022: 17th European Conference, Tel Aviv, Israel, October 23–27, 2022, Proceedings, Part XXXIII*, page 709–727, Berlin, Heidelberg, 2022. Springer-Verlag. 3
- [27] Sanghyeon Kim, Hyunmo Yang, Younghyun Kim, Youngjoon Hong, and Eunbyung Park. Corrigendum to “hydra: Multi-head low-rank adaptation for parameter efficient fine-tuning” [neural networks volume 178, october (2024), 1-11/106414]. *Neural Networks*, 181:106878, 2025. 3
- [28] Go-Eun Lee, Seon Ho Kim, Jungchan Cho, Sang Tae Choi, and Sang-II Choi. Text-guided cross-position attention for segmentation: Case of medical image. In *International Conference on Medical Image Computing and Computer-Assisted Intervention*, pages 537–546. Springer, 2023. 2
- [29] Vladislav Lialin, Vijeta Deshpande, and Anna Rumshisky. Scaling down to scale up: A guide to parameter-efficient fine-tuning, 03 2023. 3
- [30] Ilya Loshchilov and Frank Hutter. Decoupled weight decay regularization. *arXiv preprint arXiv:1711.05101*, 2017. 5
- [31] Yunyao Lu, Yihang Wu, Reem Kateb, and Ahmad Chad-dad. Semi-supervised medical image segmentation via dual networks. In *2025 IEEE 22nd International Symposium on Biomedical Imaging (ISBI)*, pages 1–5. IEEE, 2025. 1
- [32] Timo Lüddecke and Alexander Ecker. Image segmentation using text and image prompts. In *Proceedings of the IEEE/CVF conference on computer vision and pattern recognition*, pages 7086–7096, 2022. 2, 4, 7, 8
- [33] Shu Manli, Nie Weili, Huang De-An, Yu Zhiding, Gold-stein Tom, Anandkumar Anima, and Xiao Chaowei. Test-time prompt tuning for zero-shot generalization in vision-language models. In *NeurIPS*, 2022. 3
- [34] Phan Ngoc Lan, Nguyen Sy An, Dao Viet Hang, Dao Van Long, Tran Quang Trung, Nguyen Thi Thuy, and Dinh Viet Sang. Neounet: Towards accurate colon polyp segmentation and neoplasm detection. In *Advances in visual computing: 16th international symposium, ISVC 2021, virtual event, October 4-6, 2021, proceedings, part II*, pages 15–28. Springer, 2021. 5, 7, 8
- [35] Zizheng Pan, Bohan Zhuang, Haoyu He, Jing Liu, and Jian-fei Cai. Less is more: Pay less attention in vision transformers. In *Proceedings of the AAAI conference on artificial intelligence*, volume 36, pages 2035–2043, 2022. 5
- [36] Theodoros Panagiotakopoulos, Pier Luigi Dovesi, Linus Härenstam-Nielsen, and Matteo Poggi. Online domain adaptation for semantic segmentation in ever-changing conditions. In *Computer Vision – ECCV 2022: 17th European Conference, Tel Aviv, Israel, October 23–27, 2022, Proceedings, Part XXXIV*, page 128–146, Berlin, Heidelberg, 2022. Springer-Verlag. 3
- [37] Jonas Pfeiffer, Aishwarya Kamath, Andreas Rücklé, Kyunghyun Cho, and Iryna Gurevych. AdapterFusion: Non-destructive task composition for transfer learning. In Paola Merlo, Jorg Tiedemann, and Reut Tsarfay, editors, *Proceedings of the 16th Conference of the European Chapter of the Association for Computational Linguistics: Main Volume*, pages 487–503, Online, Apr. 2021. Association for Computational Linguistics. 3
- [38] Kanchan Poudel, Manish Dhakal, Prasiddha Bhandari, Rabin Adhikari, Safal Thapaliya, and Bishesh Khanal. Exploring transfer learning in medical image segmentation using vision-language models. *arXiv preprint arXiv:2308.07706*, 2023. 5
- [39] Alec Radford, Jong Wook Kim, Chris Hallacy, Aditya Ramesh, Gabriel Goh, Sandhini Agarwal, Girish Sastry, Amanda Askell, Pamela Mishkin, Jack Clark, et al. Learning transferable visual models from natural language supervision. In *International conference on machine learning*, pages 8748–8763. PmLR, 2021. 2
- [40] Vibashan VS, Poojan Oza, and Vishal M. Patel. Towards online domain adaptive object detection. In *Proceedings of the IEEE/CVF Winter Conference on Applications of Computer Vision (WACV)*, pages 478–488, January 2023. 3
- [41] Risheng Wang, Tao Lei, Ruixia Cui, Bingtao Zhang, Hongying Meng, and Asoke K. Nandi. Medical image segmentation using deep learning: A survey. *IET Image Processing*, 16(5):1243–1267, Jan. 2022. 1
- [42] Zhaoqing Wang, Yu Lu, Qiang Li, Xunqiang Tao, Yandong Guo, Mingming Gong, and Tongliang Liu. Cris: Clip-driven referring image segmentation. In *Proceedings of the IEEE/CVF conference on computer vision and pattern recognition*, pages 11686–11695, 2022. 2, 7, 8
- [43] Zifeng Wang, Zhenbang Wu, Dinesh Agarwal, and Jimeng Sun. Medclip: Contrastive learning from unpaired medical images and text. In *Proceedings of the Conference on Empirical Methods in Natural Language Processing. Conference on Empirical Methods in Natural Language Processing*, volume 2022, page 3876, 2022. 2
- [44] Zifeng Wang, Zhenbang Wu, Dinesh Agarwal, and Jimeng Sun. MedCLIP: Contrastive learning from unpaired medical images and text. In Yoav Goldberg, Zornitsa Kozareva, and Yue Zhang, editors, *Proceedings of the 2022 Conference on Empirical Methods in Natural Language Processing*, pages 3876–3887, Abu Dhabi, United Arab Emirates, Dec. 2022. Association for Computational Linguistics. 2
- [45] Xiaobao Wei, Jiajun Cao, Yizhu Jin, Ming Lu, Guangyu Wang, and Shanghang Zhang. I-medsam: Implicit med-

- ical image segmentation with segment anything. In Aleš Leonardis, Elisa Ricci, Stefan Roth, Olga Russakovsky, Torsten Sattler, and Gül Varol, editors, *Computer Vision – ECCV 2024*, pages 90–107, Cham, 2025. Springer Nature Switzerland. 3, 7, 8
- [46] Mengde Xu, Zheng Zhang, Fangyun Wei, Han Hu, and Xiang Bai. Side adapter network for open-vocabulary semantic segmentation. In *Proceedings of the IEEE/CVF Conference on Computer Vision and Pattern Recognition (CVPR)*, pages 2945–2954, June 2023. 7, 8
- [47] Jingwen Ye, Ruonan Yu, Songhua Liu, and Xinchao Wang. Mutual-modality adversarial attack with semantic perturbation. *Proceedings of the AAAI Conference on Artificial Intelligence*, 38(7):6657–6665, Mar. 2024. 2
- [48] Seonghoon Yu, Paul Hongsuck Seo, and Jeany Son. Zero-shot referring image segmentation with global-local context features. In *Proceedings of the IEEE/CVF conference on computer vision and pattern recognition*, pages 19456–19465, 2023. 2
- [49] Tao Yu, Zhihe Lu, Xin Jin, Zhibo Chen, and Xinchao Wang. Task residual for tuning vision-language models. In *Proceedings of the IEEE/CVF Conference on Computer Vision and Pattern Recognition*, pages 10899–10909, 2023. 2
- [50] Jianpeng Zhang, Yutong Xie, Yong Xia, and Chunhua Shen. Dodnet: Learning to segment multi-organ and tumors from multiple partially labeled datasets. In *Proceedings of the IEEE/CVF conference on computer vision and pattern recognition*, pages 1195–1204, 2021. 1
- [51] Qingru Zhang, Minshuo Chen, Alexander Bukharin, Pengcheng He, Yu Cheng, Weizhu Chen, and Tuo Zhao. Adaptive budget allocation for parameter-efficient fine-tuning. In *The Eleventh International Conference on Learning Representations*, 2023. 3
- [52] Shijun Zhang, Jianfeng Lu, and Hongkai Zhao. Deep network approximation: Beyond relu to diverse activation functions. *Journal of Machine Learning Research*, 25(35):1–39, 2024. 4
- [53] Sheng Zhang, Yanbo Xu, Naoto Usuyama, Hanwen Xu, Jaspreet Bagga, Robert Tinn, Sam Preston, Rajesh Rao, Mu Wei, Naveen Valluri, Cliff Wong, Andrea Tupini, Yu Wang, Matt Mazzola, Swadheen Shukla, Lars Liden, Jianfeng Gao, Angela Crabtree, Brian Piening, Carlo Bifulco, Matthew P. Lungren, Tristan Naumann, Sheng Wang, and Hoifung Poon. A multimodal biomedical foundation model trained from fifteen million image–text pairs. *NEJM AI*, 2(1), 2024. 2
- [54] Youshan Zhang. A survey of unsupervised domain adaptation for visual recognition. *CoRR*, abs/2112.06745, 2021. 3
- [55] Zihao Zhao, Yuxiao Liu, Han Wu, Mei Wang, Yonghao Li, Sheng Wang, Lin Teng, Disheng Liu, Zhiming Cui, Qian Wang, et al. Clip in medical imaging: A comprehensive survey. *arXiv preprint arXiv:2312.07353*, 2023. 2
- [56] Yuan Zhong, Chenhui Tang, Yumeng Yang, Ruoxi Qi, Kang Zhou, Yuqi Gong, Pheng-Ann Heng, Janet H. Hsiao, and Qi Dou. Weakly-supervised Medical Image Segmentation with Gaze Annotations. In *proceedings of Medical Image Computing and Computer Assisted Intervention – MICCAI 2024*, volume LNCS 15003. Springer Nature Switzerland, October 2024. 1
- [57] Ziqin Zhou, Yinjie Lei, Bowen Zhang, Lingqiao Liu, and Yifan Liu. Zegclip: Towards adapting clip for zero-shot semantic segmentation. In *Proceedings of the IEEE/CVF conference on computer vision and pattern recognition*, pages 11175–11185, 2023. 2
- [58] Yang Zou, Zhiding Yu, Xiaofeng Liu, B. V. K. Vijaya Kumar, and Jinsong Wang. Confidence regularized self-training. In *2019 IEEE/CVF International Conference on Computer Vision (ICCV)*, pages 5981–5990, 2019. 3